

Concentration field in traveling-wave and stationary convection in fluid mixtures

K. D. Eaton, Daniel R. Ohlsen,* S. Y. Yamamoto, and C. M. Surko

Department of Physics and Institute for Nonlinear Science, University of California at San Diego, La Jolla, California 92093

W. Barten and M. Lücke

Institut für Theoretische Physik, Universität des Saarlandes, D-6600 Saarbrücken, Federal Republic of Germany

M. Kamps

Stabstelle Supercomputing, Forschungszentrum Jülich, D-5170 Jülich, Federal Republic of Germany

Paul Kolodner

AT&T Bell Laboratories, Murray Hill, New Jersey 07974

(Received 30 January 1991)

By comparison of measurements of shadowgraph images of convection in ethanol-water mixtures with the results of recent numerical calculations, we study the role of the concentration field in traveling-wave and stationary convection. The results confirm the existence of a large concentration contrast between adjacent traveling-wave convection rolls. This concentration modulation, which decreases as the Rayleigh number is increased and the transition to stationary convection is approached, is fundamental to the translation of the pattern.

In the past several years, there has been considerable interest in the patterns and dynamics associated with convection in fluid mixtures.¹⁻⁵ Interest is sparked by the fact that, in mixtures such as ethanol and water, the first bifurcation can be to a stable state of traveling waves (TW). The coexisting, unstable state of stationary convection becomes stable only at larger thermal stress, when the TW frequency has decreased to zero. At this point, the stationary state is stabilized by a transition which restores the mirror symmetry of the concentration field about the upflow and downflow roll boundaries which is absent in the TW state. Since the fluid equations are well known and the boundary conditions of the system can be precisely controlled, one has a nearly ideal nonequilibrium system in which to study different patterns, their dynamics, and transitions between them.

Experimental study of these patterns has almost exclusively relied on shadowgraph techniques, where variations in the index of refraction are imaged.¹ In this paper we present precise measurements of the shadowgraph intensity, and we compare them with numerical calculations. We show that one can distinguish contributions to the optical signal due to concentration from those due to temperature. Thus we are able to study the concentration field as a function of Rayleigh number and to study the dependence of the form, symmetry, and phasing of the concentration field relative to the temperature field as the transition from TW to stationary convection is approached. Much of the significance of this study is due to the prediction, which we confirm in this paper, that the phasing of the concentration field relative to the temperature and velocity fields determines whether or not the pattern propagates.

In a binary fluid mixture, the separation ratio ψ , which is proportional to the Soret coefficient, parametrizes temperature-driven concentration variations.¹ For $\psi < 0$,

the lighter component diffuses toward the colder region, thereby stabilizing the fluid layer against convection, and the Rayleigh number at onset is larger than that for a pure fluid. In this Rapid Communication, all Rayleigh numbers r will be normalized by the onset Rayleigh number, R_c^0 , of convection in a pure fluid with the same thermal properties as those of the mixture.

The experiments are conducted in a long, narrow annular cell with a rectangular cross section. In this geometry, the roll axes are oriented radially, and the boundary conditions are periodic in the (azimuthal) direction of TW propagation. The apparatus is described in Ref. 5. The convection cell has a copper bottom plate and a sapphire top plate. The vertical walls are machined plastic with a height of $d = 0.309 \pm 0.002$ cm. The cell dimensions are, in units of d , 1.288 in width by 67.09 in mean circumference. The working fluid is a mixture of 8.00% by weight ethanol in water. The top-plate temperature is fixed at 25.00°C and regulated to ± 0.7 mK, and the bottom-plate temperature varies from 29.6 to 32.0°C with similar regulation. At the onset of convection, where the average temperature is 27.53°C, the fluid parameters are $\psi = -0.26$, $P = 9.16$, and $L = 0.008$,⁵ where P and L are the Prandtl and Lewis numbers, respectively.

The flow is visualized from above with the shadowgraph method.⁶ The shadowgraph image is recorded with a 720-element circular photodiode array, which corresponds to a spatial resolution of approximately $0.1d$. The radial extent of the photodiode elements is larger than that of the image. Care is taken to ensure that the intensity pattern is recorded at a position where the spatial modulation in the optical intensity $I(x)$ is in the linear regime.⁶ In this case,

$$I(x) = A \frac{\partial^2}{\partial x^2} [\bar{c}(x) + b\bar{\theta}(x)], \quad (1)$$

where A is a constant, and $\bar{c}(x)$ and $\bar{\theta}(x)$ are vertical averages of the convection-induced modulations in the concentration and temperature fields, $C(x, z)$ and $T(x, z)$, with x the azimuthal and z the vertical direction.⁶ In Eq. (1), $b = -0.919$ for the fluid described above, using the units of C and T given in Refs. 3 and 4.

Convection is observed to begin at a Rayleigh number $r_{co} = 1.80$ with a subcritical Hopf bifurcation. This evolves to a stable nonlinear TW state with a frequency ω , which is approximately 45 times smaller than the Hopf frequency at the same Rayleigh number.⁵ If r is decreased, TW convection persists with ω increasing by about a factor of 10 until a saddle-node bifurcation is reached at a Rayleigh number $r_s = 1.62$. At r_s , a transition to the (quiescent) conductive state occurs. For $r > r_s$ in the convecting state, as r is raised, ω decreases to $\omega = 0$ at a Rayleigh number $r^* = 1.83$. At this point, the system undergoes a transition to stable, stationary overturning convection (SOC).

Finite-difference numerical calculations have been carried out for fluid parameters similar to those of the experimental mixture ($\psi = -0.25$, $P = 10$, $L = 0.01$). The calculations are performed on a uniform grid of spacing $0.05d$. They assume the Oberbeck-Boussinesq approximation of the fluid equations, two-dimensional flow perpendicular to the roll axes, rigid impermeable boundary conditions at the upper and lower plates of the container, and periodic boundary conditions with wavelength $\lambda = 2d$ in the other dimension. These calculations reproduce the features of the TW and SOC states observed in the experiments.⁵ The major quantitative discrepancies are that, experimentally, convection requires larger thermal driving, and the range of Rayleigh numbers over which TWs are observed is smaller than in the numerical calculations [i.e., $r_{co} = 1.33$ (1.80), $r_s = 1.21$ (1.62), and $r^* = 1.65$ (1.83) for the calculations (experiment)].⁷

The calculated, vertically integrated fields were convolved with a square window of width $0.1d$, which is two times the numerical grid spacing and approximately equal to the resolution of the photodiode array. The results for \bar{c} and $\bar{\theta}$ are shown in Fig. 1 for a TW just above r_s and an SOC state above r^* . As shown in Fig. 1(c), the calculations indicate that, in a TW, there is a difference in the concentration between adjacent left- and right-turning rolls, while the concentration within a roll is approximately constant. Thus the concentration is uniform, except in the upflow and downflow roll boundaries and in the boundary layers near the upper and lower plates. The concentration contrast between the rolls is largest near r_s and decreases continuously to zero, as does ω , as r is increased to r^* .^{3,4} The widths of the boundary layers near the plates and between the rolls shrink, albeit not to zero. In the TW to SOC transition at r^* , the mirror symmetry between left- and right-turning rolls is restored. Thereafter, the concentration field is almost perfectly homogeneous laterally, except for a mirror-symmetric variation in the upflow and downflow boundaries between the rolls.

The quantities $\partial_x^2 \bar{\theta}$ and $\partial_x^2 \bar{c}$ are shown in Figs. 1(b) and 1(d), where x has been scaled by the cell height d . The optical signal, $I(x)$, is shown in Fig. 1(e). In this paper, the numerical optical signals are plotted using Eq. (1)

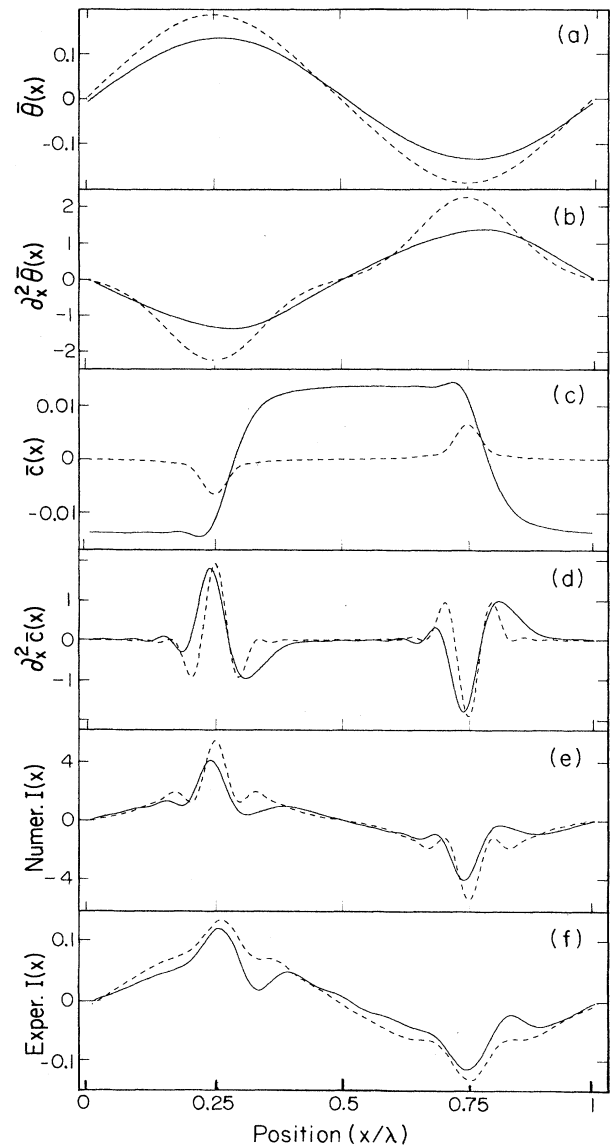


FIG. 1. The numerically calculated, vertically averaged temperature and concentration modulations, $\bar{\theta}$ and \bar{c} , are plotted in (a) and (c) as a function of horizontal position across a roll pair. Shown is a right-moving traveling wave just above r_s at $r = 1.25$ (solid lines) and an SOC state at $r = 1.82$ (dashed lines). The second spatial derivatives, $\partial_x^2 \bar{\theta}$ and $\partial_x^2 \bar{c}$, are plotted in (b) and (d), and the predicted optical signals are shown in (e). Shown in (f) are the experimental optical signals just above r_s at $r = 1.64$ (solid line), and just above r^* at $r = 1.87$ (dashed line).

with $A = 1$. As shown in Fig. 1, in a TW there is a phase shift between the main peak in $\partial_x^2 \bar{c}$ [and $I(x)$] and the extrema of $\partial_x^2 \bar{\theta}$. This shift, and the one between the temperature and vertical velocity,^{3,4} vanishes at the TW-SOC transition. The calculated temperature and concentration fields of SOC and TW states are both symmetric under lateral translation by half a wavelength and subsequent reflection at the horizontal midplane of the fluid layer,^{3,4} but the mirror symmetry of left- and right-turning rolls is broken in a TW. Thus the optical signal of a TW shows

the symmetry $I(x+\lambda/2) = -I(x)$, but not mirror symmetry around upflow and downflow boundaries that characterizes a SOC state [i.e., $I(x_0+x) = I(x_0-x)$, where x_0 is the position of a roll boundary]. This is illustrated in Figs. 1(e) and 1(f), where the positive (negative) peaks of $I(x)$ mark the upflows (downflows).

Shown in Fig. 1(f) is the measured shadowgraph intensity at Rayleigh numbers just above r_s and just above r^* . The finite size of the detector elements limits our spatial resolution. In order to improve the signal, the data were taken as the patterns propagate past the stationary detector elements. The optical signals at ten different times were phased and averaged. The averaged data were typically separated into six single-wavelength segments, scaled to correct for a small but non-negligible wavelength variation across the cell, and then averaged. The experimental optical signals plotted are in units such that 0.1 corresponds to 10% greater light intensity than when no convection is present. The average value of the rms error is 0.004, corresponding to a typical rms error of 10%. As described above, the $\partial_x^2 \bar{\theta}$ contribution to the optical signal is smooth, nearly sinusoidal, and almost symmetric about upflow and downflow boundaries; whereas the $\partial_x^2 \bar{c}$ contribution has sharp features, and, in a TW state, it is asymmetric about these boundaries. These features allow us to distinguish the component of the optical signal due to concentration from that due to temperature in the experimen-

tal optical signals.⁸

Given that, to within our experimental accuracy, the measured signals show the symmetry $I(x+\lambda/2) = -I(x)$, in Fig. 2 we compare the calculations and experiment for different Rayleigh numbers between r_s and r^* by averaging the data from two half periods with the negative half period inverted. The mirror asymmetry of the TW about the roll boundary is clearly visible as is the decrease in this asymmetry as the Rayleigh number is increased. The intensity of the primary peak increases with r and moves to the right, reflecting the decreasing phase difference^{3,4} between \bar{c} and $b\bar{\theta}$. The side peaks move inward, and their height increases as the upflow and downflow concentration boundary layers shrink. One difference between the calculations and experiment is that the calculations show a small peak to the left of the main peak, while the experimental signals indicate only a shoulder.

Shown in Fig. 3(a) is the numerically calculated optical signal and its two components, $b\partial_x^2 \bar{\theta}$ and $\partial_x^2 \bar{c}$, for an SOC state above r^* . The temperature component, $b\partial_x^2 \bar{\theta}$, is nearly identical to that for a pure fluid with the same fluid parameters. The sharp features in $\partial_x^2 \bar{c}$ produce correspondingly sharp features in $I(x)$, which are now symmetric about the roll boundary. Shown in Fig. 3(b) is the experimental optical signal for a state with $r > r^*$. States with a small but finite speed (~ 100 times smaller than speeds for $r < r^*$) are sometimes observed⁵ above r^* , and they were used to create the temporally and spatially averaged optical signal shown in Fig. 3(b). The characteristic

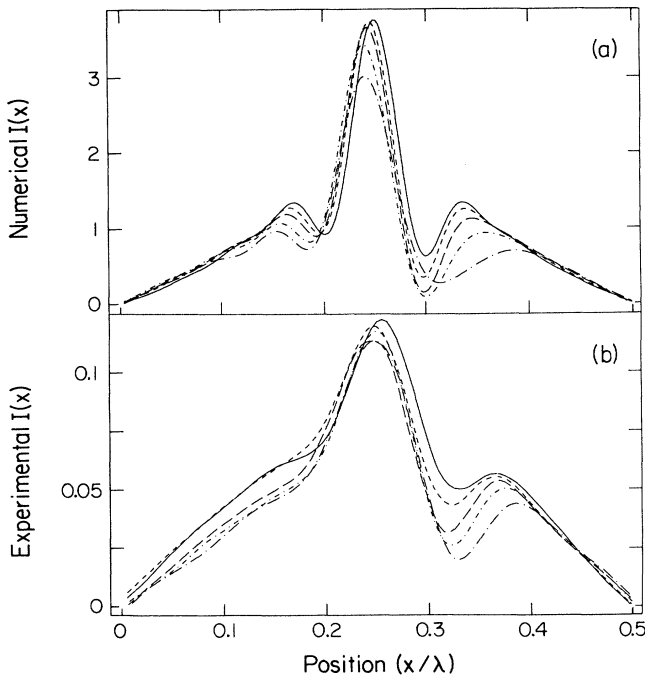


FIG. 2. Optical signals for right-moving TW states for $r_s < r < r^*$. In (a), numerical results are presented for $r=1.62$ (solid line), $r=1.52$ (short-dashed line), $r=1.42$ (long-dashed line), $r=1.32$ (dot-short-dashed line), and $r=1.25$ (dot-long-dashed line). In (b), experimental signals are shown for $r=1.78$ (solid line), $r=1.74$ (short-dashed line), $r=1.71$ (long-dashed line), $r=1.67$ (dot-short-dashed line), and $r=1.64$ (dot-long-dashed line).

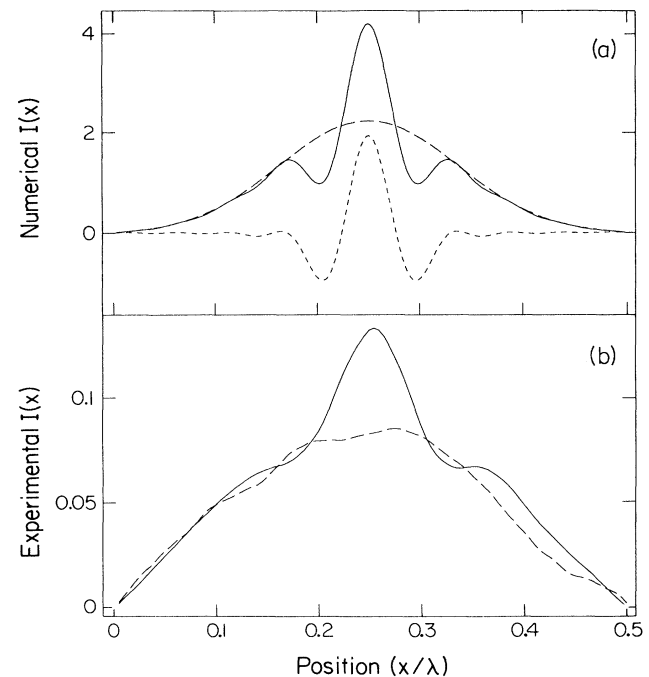


FIG. 3. (a) Numerical calculations for the optical signal, $I(x)$ (solid line), $\partial_x^2 \bar{c}$ (short-dashed line), and $b\partial_x^2 \bar{\theta}$ (long-dashed line) for an SOC state at $r=2.03$. (b) The experimentally observed optical signals for the fluid mixture at $r=1.87$ (solid line), which corresponds to $r > r^*$, and for pure fluid convection at $r=1.74$ (dashed line).

asymmetry observed below r^* is absent. Also shown in Fig. 3(b) is the shadowgraph image of water (i.e., a pure fluid) at $r = 1.74$. In this case, the data are noisier, but the concentration feature is clearly absent. As shown in Figs. 1(b) and 3(a), near r^* , the calculations for $\partial_x^2 \bar{\theta}$ have significant contributions from the third harmonic which appears to be absent in the experimental data. This may be due to the fact that the calculations assume a two-dimensional flow, while the experiment measures the spatial integral over a sidewall-influenced three-dimensional flow.

In this paper, we have shown that the concentration field in convection in fluid mixtures can be studied using a combination of shadowgraph measurements and numerical calculations. We confirm the predicted form, symme-

try, and phasing of the TW concentration field and the existence of a concentration contrast between adjacent rolls, which decreases with increasing Rayleigh number and vanishes at the TW-SOC transition. This study and related work³⁻⁵ place our understanding of the simplest states of TW convection in mixtures on a firm and quantitative basis.

We wish to acknowledge helpful discussions from and the assistance of G. W. Baxter. This work was supported by the Department of Energy under Grant No. DE-FG03-90ER14148, the Defense Advanced Research Projects Agency University Research Initiative Contract No. N00014-86-K-0758, and the Deutsche Forschungsgemeinschaft.

*Present address: School of Oceanography, University of Washington, Seattle, WA 98195.

¹P. Kolodner, C. M. Surko, and H. Williams, *Physica D* **37**, 319 (1989); R. Heinrichs, G. Ahlers, and D. S. Cannell, *Phys. Rev. A* **35**, 2761 (1987); E. Moses, J. Fineberg, and V. Steinberg, *ibid.* **35**, 2757 (1987); D. Bensimon, P. Kolodner, and C. M. Surko, *J. Fluid Mech.* **217**, 441 (1990).

²D. Bensimon, B. I. Shraiman, and V. Croquette, *Phys. Rev. A* **38**, 5461 (1988); S. Fauve and O. Thual, *Phys. Rev. Lett.* **64**, 282 (1990); W. van Saarloos and P. C. Hohenberg, *ibid.* **64**, 749 (1990).

³W. Barten, M. Lücke, W. Hort, and M. Kamps, *Phys. Rev. Lett.* **63**, 376 (1989).

⁴W. Barten, M. Lücke, and M. Kamps, in *Non-Linear Evolution of Spatiotemporal Structures*, edited by F. H. Busse and L. Kramer, NATO Advanced Study Institutes Ser. B2 Vol. 225 (Plenum, New York, 1990), p. 131.

⁵D. R. Ohlsen, S. Y. Yamamoto, C. M. Surko, and P. Kolodner,

Phys. Rev. Lett. **65**, 1431 (1990); *J. Stat. Phys.* (to be published).

⁶V. Croquette, *Contemp. Phys.* **30**, 113 (1988); S. Rasenat, G. Hartung, B. L. Winkler, and I. Rehberg, *Exp. Fluids* **7**, 412 (1989).

⁷The measured values of r_s and r_{co} are both larger than those predicted by the (two-dimensional) numerical calculations. They do, however, appear to obey the same empirical scaling with finite channel width that is observed for the onset of convection in pure fluids. In contrast, r^* is very similar in experiment and the numerical calculations. We know of no physical model for the dependence of r^* on channel width.

⁸In principle, the concentration field can be obtained from $I(x)$ by subtracting the temperature component and integrating twice. (For $r \gtrsim r^*$, the temperature component is approximately that of a pure fluid at the same r .) We attempted this, but were unable to recover the \bar{c} field due to the sensitivity to the amplitude and phasing of the signals.